Quantum and Semiclassical Stark Widths for Ar VII Spectral Lines

Rihab Aloui [1], **Haykel Elabidi** [2,*] , **Sylvie Sahal-Bréchot** [3] and **Milan S. Dimitrijević** [3,4,†]

[1] Laboratoire Dynamique Moléculaire et Matériaux Photoniques, GRePAA, École Nationale Supérieure d'ingénieurs de Tunis, University of Tunis, 1008 Tunis, Tunisia; rihabaloui88@gmail.com

[2] LDMMP, GRePAA, Faculté des Sciences de Bizerte, University of Carthage, 7021 Bizerte, Tunisia

[3] Sorbonne Université, Observatoire de Paris, Université PSL, CNRS, LERMA, F-92190 Meudon, France; sylvie.sahal-brechot@obspm.fr (S.S.-B.); mdimitrijevic@aob.rs (M.S.D.)

[4] Astronomical Observatory, Volgina 7, 11060 Belgrade, Serbia

* Correspondence: haelabidi@uqu.edu.sa; Tel.: +966-564-518-933

† Current address: Astronomical Observatory, Volgina 7, 11060 Belgrade, Serbia.

Abstract: We present in this paper the results of a theoretical study of electron impact broadening for several lines of the Ar VII ion. The results have been obtained using our quantum mechanical method and the semiclassical perturbation one. Results are presented for electron density 10^{18} cm^{-3} and for electron temperatures ranging from 2×10^4 to 5×10^5 K required for plasma modeling. Our results have been compared to other semiclassical ones obtained using different sources of atomic data. A study of the strong collisions contributions to line broadening has been performed. The atomic structure and collision data used for the calculations of line broadening are also calculated by our codes and compared to available theoretical results. The agreement found between the two calculations ensures that our line broadening procedure uses adequate structure and collision data.

Keywords: Stark broadening; Ar VII line profiles; stars; white dwarfs; atomic data; scattering

1. Introduction

Atomic and line broadening data for many elements and their ions are very useful for solving many astrophysical problems, such as the calculations of opacity and radiative transfer [1]. Especially, accurate Stark broadening parameters are important to obtain a reliable modelization of stellar interiors. The Stark broadening mechanism is also important for the investigation, analysis, and modeling of B-type and particularly A-type stellar atmospheres, as well as white dwarf atmospheres [2,3]. Furthermore, the development of computers and instruments, such as the new X-ray space telescope *Chandra*, has motivated the calculations of line broadening of trace elements in the X-ray wavelength range. It has been shown that analysis of white dwarf atmospheres, where Stark broadening is dominant compared to the thermal Doppler broadening, needs models taking into account heavy element opacity.

In Rauch et al. [4], the authors reported problems encountered in their determination of element abundances: the line cores of the S VI resonance doublet appear too deep to match the observation and they are not well suited for an abundance determination, and the same problem exists in relation to the N V and O VI. This is due to the lack of line broadening data for these ions. Some other data exist, but the required temperatures and electron densities are lacking, and it is necessary to extrapolate such data to obtain the temperatures and densities at the line-forming regions, especially the line cores. This procedure of extrapolation can provide inaccurate results especially in the case of extrapolating to obtain temperatures, since the temperature dependence of line widths may be very different. This lack

of data represents an inconvenience for the development of spectral analysis by means of the NLTE model atmosphere techniques. We quote here the conclusion in Rauch et al. [4]: "spectral analysis by means of NLTE model atmospheres has presently arrived at a high level of sophistication, which is now hampered largely by the lack of reliable atomic data and accurate line-broadening tables."

Astrophysical interest of Ar VII illustrates for example recent discovery of far UV lines of this ion in the spectra of very hot central stars of planetary nebulae and white dwarfs [5]. In this article, the authors have also shown the importance of the line broadening data for this element in its various ionization stages. Argon also has an important role in plasma technological applications and devices [6]. It produces favorable conditions for very stable discharges and is also very often used as a carrier gas in plasma, which contains a mixture of other gases. Thus, the knowledge of the Stark broadening parameters of neutral and ionized argon lines is an important tool for plasma electron density diagnostic.

The Stark broadening calculations in the present work are based on two approaches: the quantum mechanical approach and the semiclassical perturbation one. The quantum mechanical expression for electron impact broadening calculations for intermediate coupling was obtained in Elabidi et al. [7]. The first applications were performed for the 2s3s−2s3p transitions in Be-like ions from nitrogen to neon [8] and for the 3s−3p transitions in Li-like ions from carbon to phosphor [9]. This approach was also used in Elabidi & Sahal-Bréchot [10] to check the dependence on the upper level ionization potential of electron impact widths and in Elabidi et al. [11] to investigate the influence of strong collisions and quadrupolar potential contributions on line broadening. Our quantum approach is an ab initio method; i.e., all the parameters required for the calculations of the line broadening such as radiative atomic data (energy levels, oscillator strengths ...) or collisional data (collision strengths or cross sections, scattering matrices ...) are evaluated during the calculation and not taken from other data sources. We used the sequence of the University College London (UCL) atomic codes SUPERSTRUCTURE/DW/JAJOM that have been used for many years to provide fine energy levels, wavelengths, radiative probability rates, and electron impact collision strengths. Recently, they have been adapted to line broadening calculations [8].

In the present paper, we continue the effort to provide atomic and line broadening data for argon ions. Quantum Stark broadening of 12 lines of the Ar VII ion have been calculated using 9 configurations ($1s^2 2s^2 2p^6$: $3s^2$, 3s3p, $3p^2$, 3s3d, 3p3d, 3s4s, 3s4p, 3s4d, and 3s5s). Our calculations have been made for a set of temperatures ranging from 2×10^4 to 5×10^5 K. These parameters will be useful for a more accurate determination of photospheric properties. We perform also a semiclassical calculations for these lines using our atomic data from the code SUPERSTRUCTURE. We compare these results to the semiclassical ones [12], for which the atomic structure has been calculated with the Bates and Damgaard approximation [13].

2. Outline of the Theory and Computational Procedure

2.1. Quantum Mechanical Formalism

We present here an outline of our quantum formalism for electron impact broadening. More details can be found elsewhere [7,8]. The calculations are made within the frame of the impact approximation, which means that the time interval between collisions is much longer than the duration of a collision. The expression of the Full Width at Half Maximum (FWHM) W obtained in Elabidi et al. [8] is:

$$
\begin{aligned}
W \;=\; & 2N_e \left(\frac{\hbar}{m}\right)^2 \left(\frac{2m\pi}{k_B T}\right)^{\frac{1}{2}} \\
& \times \int_0^\infty \Gamma_w(\varepsilon) \exp\left(-\frac{\varepsilon}{k_B T}\right) d\left(\frac{\varepsilon}{k_B T}\right)
\end{aligned}
\tag{1}
$$

where k_B is the Boltzmann constant, N_e the electron density, T the electron temperature, and

$$\Gamma_w(\varepsilon) \;=\; \sum_{J_i^T J_f^T l K_i K_f} \frac{\left[K_i, K_f, J_i^T, J_f^T\right]}{2}$$

$$\times \left\{ \begin{array}{c} J_i K_i l \\ K_f J_f 1 \end{array} \right\}^2 \left\{ \begin{array}{c} K_i J_i^T s \\ J_f^T K_f 1 \end{array} \right\}^2$$

$$\times \left[1 - \left(\mathrm{Re}\,(S_I)\mathrm{Re}\,(S_F) + \mathrm{Im}\,(S_I)\mathrm{Im}\,(S_F)\right)\right] \tag{2}$$

where $L_i + S_i = J_i$, $J_i + l = K_i$ and $K_i + s = J_i^T$. L and S represent the atomic orbital angular momentum and spin of the target, l is the electron orbital momentum, and the superscript T denotes the quantum numbers of the total electron+ion system. S_I (S_F) are the scattering matrix elements for the initial (final) levels, expressed in the intermediate coupling approximation, Re (S) and Im (S) are respectively the real and the imaginary parts of the S-matrix element, $\left\{ \begin{array}{c} abc \\ def \end{array} \right\}$ represent 6–j symbols, and we adopt the notation $[x, y] = (2x + 1)(2y + 1)$. Both S_I and S_F are calculated for the same incident electron energy $\varepsilon = mv^2/2$. Equation (1) takes into account the fine structure effects and relativistic corrections resulting from the breakdown of the *LS* coupling approximation for the target.

The main goal is the evaluation of the real (Re **S**) and the imaginary parts (Im **S**) of the scattering matrix **S** in the initial I and the final F level. The calculation starts with the study of the atomic structure. The structure problem has been treated using the SUPERSTRUCTURE (SST) code described in Eissner et al. [14], taking into account configuration interaction, where each individual configuration is an expansion in terms of Slater states built from orthonormal orbitals. The radial functions were calculated assuming a scaled Thomas–Fermi–Dirac–Amaldi (TFDA) potential. The potential depends upon parameters λ_l which are determined variationally by optimizing the weighted sum of the term energies. Relativistic corrections (spin-orbit, mass, Darwin, and one-body) are introduced according to the Breit–Pauli approach [15] as a perturbation to the non-relativistic Hamiltonian. The SST program also produces the term coupling coefficients (TCCs), which are used to transform the scattering **S** or reactance **R**-matrices to intermediate coupling [7].

The second step is the treatment of the scattering problem. The calculation is carried out in the non-relativistic distorted wave approximation using the UCL distorted wave (DW) program [16]. The reactance matrices are calculated in LS coupling. The program JAJOM [17] uses these reactance matrices and the TCC to calculate collision strengths in intermediate coupling. In the present work, we have transformed JAJOM into JAJPOLARI (Elabidi and Dubau, unpublished results) to produce the collision strengths and the reactance matrices **R** in intermediate coupling, which will be used by the program RtoS (Dubau, unpublished results) to evaluate the real and the imaginary parts of the scattering matrix according to

$$\mathrm{Re}\,\mathbf{S} = \left(1 - \mathbf{R}^2\right)\left(1 + \mathbf{R}^2\right)^{-1} \tag{3}$$

and

$$\mathrm{Im}\,\mathbf{S} = 2\mathbf{R}\left(1 + \mathbf{R}^2\right)^{-1}. \tag{4}$$

The two expressions (3) and (4) have been deduced from the relation $\mathbf{S} = (\mathbf{1} + i\mathbf{R})(\mathbf{1} - i\mathbf{R})^{-1}$, and such expressions guarantee the unitarity of the **S**-matrix.

Finally, in the code JAJPOLARI, the reactance matrices R_I in intermediate coupling corresponding to the initial I level are evaluated for each channel and at a total energy $E_I = E_i + \varepsilon$. The same procedure is done for R_F but at a total energy $E_F = E_f + \varepsilon$. E_i (E_f) are the energies of the initial (final) atomic levels. The program RtoS receives **R**-matrices and transforms them into real and imaginary parts of **S**-matrices according to Equations (3) and (4) at total energies E_I and E_F, and combines a given matrix element S_I for an initial level I with a number of matrix element S_F for the final level F. The obtained matrix elements Re **S** and Im **S** enter into Equation (2).

The integral over the Maxwell distribution (Equation (1)) is evaluated numerically using a trapezoid integration with a variable step to provide the line width W. The energy step is chosen to be as small as possible around the threshold region where the variation of Γ_w in (1) is fast. For large energies and far from the threshold region, the variation of Γ_w becomes slow and then the step is gradually increased.

2.2. Semiclassical Perturbation Method

We give here a detailed description of the semiclassical perturbation formalism for line broadening calculations. The profile $F(\omega)$ is Lorentzian for isolated lines:

$$F(\omega) = \frac{w/\pi}{(\omega - \omega_{if} - d)^2 + w^2} \tag{5}$$

where

$$\omega_{if} = \frac{E_i - E_f}{\hbar}$$

i and f denote the initial and final atomic states and E_i and E_f their corresponding energies.

The total width at half maximum ($W = 2w$) in angular frequency units of a spectral line can be expressed as

$$W = N \int v f(v) dv \left(\sum_{i' \neq i} \sigma_{ii'}(v) + \sum_{f' \neq f} \sigma_{ff'}(v) + \sigma_{el} \right) \tag{6}$$

where N is the electron density, $f(v)$ the Maxwellian velocity distribution function for electrons, i' (resp. f') denotes the perturbing levels of the initial state i (resp. final state f). The inelastic cross section $\sigma_{ii'}(v)$ (resp. $\sigma_{ff'}(v)$) can be expressed by an integral over the impact parameter ρ of the transition probability $P_{ii'}(\rho, v)$ (resp. $P_{ff'}(\rho, v)$) as

$$\sum_{i' \neq i} \sigma_{ii'}(v) = \frac{1}{2}\pi R_1^2 + \int_{R_1}^{R_D} 2\pi\rho d\rho \sum_{i' \neq i} P_{ii'}(\rho, v) \tag{7}$$

where ρ denotes the impact parameter of the incoming electron. The elastic cross section is given by

$$\sigma_{el} = 2\pi R_2^2 + \int_{R_2}^{R_D} 2\pi\rho d\rho \sin^2 \delta + \sigma_r \tag{8}$$

$$\delta = (\varphi_p^2 + \varphi_q^2)^{\frac{1}{2}}.$$

Strong collisions are evaluated for $\rho < R_1, R_2$. The phase shifts φ_p and φ_q, due respectively to the polarization potential (r^{-4}) and to the quadrupolar potential (r^{-3}), are given in Section 3 of Chapter 2 in Sahal-Bréchot [18], and R_D is the Debye radius. The cut-offs R_1 and R_2 are described in Section 1 of Chapter 3 in Sahal-Bréchot [19]. Detailed calculations of the interference term σ_{el} can be found in Formulas 18 and 24–30 on pages 109–110 of Sahal-Bréchot [18]. σ_r is the contribution of the Feshbach resonances [20], which concerns only ionized radiating atoms colliding with electrons. It is an extrapolation of the excitation collision strengths (and not the cross-sections) under the threshold by means of the semiclassical limit of the Gailitis approximation (see page 601 of [20] for details of the calculations). A review of the theory, all approximations and the details of applications are given in Sahal-Bréchot et al. [21].

3. Results and Discussions

3.1. Atomic Structure and Electron Scattering Data

We have used the following nine configurations in our calculation: $1s^2 2s^2 2p^6$: $3s^2$, $3s3p$, $3p^2$, $3s3d$, $3p3d$, $3s4s$, $3s4p$, $3s4d$, and $3s5s$, which give rise to 38 levels, which are listed in Table 1 with their energies in cm^{-1}. These values have been compared with the observed ones taken from the tables of the National Institute of Standards and Technology database: NIST [22] which are originally from Saloman [23]. We compare also with the energies computed using the multiconfiguration Hartree–Fock method (MCHF) [24] and with those obtained using the AUTOSTRUCTURE code [25]. The averaged disagreement between these three results is less than 1%. We detect an inversion between the two levels 10/13 and 25/26 regarding those of NIST and MCHF. This inversion does not affect the calculations since the agreement is still acceptable (about 5%).

Table 1. Our present fine-structure energy levels E (in cm^{-1}) for Ar VII compared with those of NIST [22], with those obtained from the multiconfiguration Hartree–Fock method (MCHF) [24], and with those from the R-matrix calculation (AS2014) [25]. Levels denoted by asterisks (*) are inverted compared to the NIST values.

i	Conf.	Level	E	NIST	MCHF	AS2014	$\frac{\lvert E-NIST \rvert}{NIST}$ (%)
1	$3s^2$	$^1S_0$	0.0	0.0	0.0	0.0	–
2	$3s3p$	$^3P^o_0$	110,717	113,101	112,817.66	112,070	2.1
3	$3s3p$	$^3P^o_1$	111,488	113,906	113,632.14	112,889	2.1
4	$3s3p$	$^3P^o_2$	113,088	115,590	115,324.84	114,593	2.2
5	$3s3p$	$^1P_1$	172,878	170,722	170,598.08	173,751	1.3
6	$3p^2$	$^1D_2$	263,439	264,749	264,797.88	264,530	0.5
7	$3p^2$	$^3P^o_0$	271,494	269,836	269,688.15	270,704	0.6
8	$3p^2$	$^3P^o_1$	272,341	270,777	270,667.14	271,641	0.6
9	$3p^2$	$^3P^o_2$	273,971	272,562	272,474.76	273,432	0.5
10	$3s3d$	$^3D_1$	325,254	324,104	324,950.35	326,054	0.4
11	$3s3d$	$^3D_2$	325,335	324,141	324,966.00	326,141	0.4
12	$3s3d$	$^3D_3$	325,456	324,205	325,056.68	326,273	0.4
13	$3p^2$	$^1S_0$	333,116	316,717	317,014.73	320,974 *	5.2
14	$3s3d$	$^1D_2$	384,031	370,294	371,275.29	377,167	3.7
15	$3p3d$	$^3F^o_2$	443,952	443,362	444,508.36	444,677	0.1
16	$3p3d$	$^3F_{3^o}$	444,892	444,780	445,556.29	445,701	0.0
17	$3p3d$	$^3F^o_4$	446,051	446,011	446,849.87	446,969	0.0
18	$3p3d$	$^1D_2$	450,025	450,477	450,808.06	451352	0.1
19	$3p3d$	$^3P^o_2$	474,314	472,282	473,009.27	475,022	0.4
20	$3p3d$	$^3P^o_1$	474,956	472,875	473,782.67	475,699	0.4
21	$3p3d$	$^3P^o_0$	475,497	473,810	474,466.36	476,301	0.4
22	$3p3d$	$^3D_1$	477,133	475,217	475,932.22	477,901	0.4
23	$3p3d$	$^3D_2$	477,515	475,585	476,306.50	478,313	0.4
24	$3p3d$	$^3D_3$	477,753	475,762	476,474.91	478,560	0.4
25	$3s4s$	$^3S_1$	513,685	514,076	508,971.69	511,372	0.1
26	$3p3d$	$^1F^o_3$	521,897	510,268	514,890.47	515,169 *	2.3
27	$3p3d$	$^1P^o_1$	527,518	517,105	517,788.24	524,282	2.0
28	$3s4s$	$^1S_0$	529,866	528,910	526,205.45	523,618	0.2
29	$3s4p$	$^3P^o_0$	567,050	563,880	568,040.66	565,087	0.6
30	$3s4p$	$^3P^o_1$	567,287	564,418	568,275.74	565,295	0.5
31	$3s4p$	$^3P^o_2$	567,811	564,728	568,944.94	565,840	0.5
32	$3s4p$	$^1P^o_1$	576,576	569,797	570,403.78	568,205	0.2
33	$3s4d$	$^3D_1$	635,209	634,605	635,580.25	632,497	0.1
34	$3s4d$	$^3D_2$	635,241	634,639	635,659.10	632,562	0.1
35	$3s4d$	$^3D_3$	635,290	634,701	635,749.02	632,659	0.1
36	$3s4d$	$^1D_2$	639,087	635,295	636,353.38	633,443	0.6
37	$3s5s$	$^3S_1$	713,912	715,747	–	717,638	0.3
38	$3s5s$	$^1S_0$	719,473	714,794	–	717,997	0.7

We present also in Table 2 radiative decay rates A_{ij}, weighted oscillator strengths gf, and line strengths S for some Ar VII lines up to the level 14 (3s3d ^{1}D$_2$). Our A_{ij} values have been compared with those obtained from the AUTOSTRUCTURE code [25], and with those from the SUPERSTRUCTURE code [26] using five configurations (1s^{2}2s^{2}2p^6: 3s^2, 3s3p, 3p^2, 3s3d, and 3s4s). The averaged difference is about 20% with the results of [25] and about 24% with those of Christensen et al. [26]. Some transitions present a high difference, especially those for which A_{i-j} are relatively small (about 10^6 s^{-1} and below). The gf values have been compared only with Christensen et al. [26] and the difference is about 24 %. The gf values are calculated in [26], but we took them from the database CHIANTI version 8.0 [27].

With the code JAJOM, fine structure collision strengths are calculated for low partial waves l of the incoming electron up to 29. For large partial waves l, this method becomes cumbersome and inaccurate, but their contributions to collision strengths cannot be neglected. For $30 \leq l \leq 50$, two different procedures have been used: for dipole transitions, the contribution has been calculated using the JAJOM-CBe code (Dubau, unpublished results) based upon the Coulomb–Bethe formulation of Burgess and Sheorey [28] and adapted to JAJOM approximation. For non-dipole transitions, the contribution has been estimated by the SERIE-GEOM code assuming a geometric series behavior for high partial wave collision strengths [29,30].

Table 2. Present radiative decay rates A_{ij} (in s^{-1}) and weighted oscillator strengths gf compared to those from Christensen et al. [26] (SST86) and to those from [25] (AS2014) for some Ar VII allowed transitions. Line strengths S are also presented. i and j label the levels as in Table 1.

$i-j$	A_{i-j}	A_{i-j}(AS2014)	A_{i-j}(SST86)	gf	gf(SST86)	S
3 − 1	5.968×10^5	7.13×10^5	1.65×10^5	2.160×10^{-4}	5.820×10^{-5}	0.000638
5 − 1	8.114×10^9	8.30×10^9	8.21×10^9	1.221×10^0	1.270×10^0	2.325423
6 − 3	1.854×10^7	2.97×10^7	2.39×10^7	6.018×10^{-3}	7.780×10^{-3}	0.013038
6 − 4	3.748×10^7	6.18×10^7	6.07×10^7	1.243×10^{-2}	2.020×10^{-2}	0.027216
6 − 5	3.719×10^8	4.00×10^8	3.98×10^8	3.400×10^{-1}	3.380×10^{-1}	1.235825
7 − 3	7.249×10^9	6.94×10^9	6.93×10^9	4.245×10^{-1}	4.280×10^{-1}	0.873472
7 − 5	7.818×10^5	1.72×10^6	1.02×10^6	1.205×10^{-4}	1.590×10^{-4}	0.000402
8 − 2	2.492×10^9	2.40×10^9	2.35×10^9	4.291×10^{-1}	4.250×10^{-1}	0.874104
8 − 3	1.842×10^9	1.77×10^9	1.74×10^9	3.202×10^{-1}	3.180×10^{-1}	0.655396
8 − 4	2.976×10^9	2.85×10^9	2.84×10^9	5.278×10^{-1}	5.310×10^{-1}	1.090986
8 − 5	1.274×10^5	1.33×10^5	3.65×10^4	5.793×10^{-5}	1.670×10^{-5}	0.000192
9 − 3	1.877×10^9	1.80×10^9	1.77×10^9	5.329×10^{-1}	5.270×10^{-1}	1.079810
9 − 4	5.481×10^9	5.24×10^9	5.22×10^9	1.587×10^0	1.590×10^0	3.248175
9 − 5	4.965×10^6	8.35×10^6	7.11×10^6	3.642×10^{-3}	5.240×10^{-3}	0.011859
10 − 2	5.993×10^9	5.86×10^9	5.92×10^9	5.857×10^{-1}	5.980×10^{-1}	0.898754
10 − 3	4.449×10^9	4.35×10^9	4.40×10^9	4.379×10^{-1}	4.480×10^{-1}	0.674448
10 − 4	2.906×10^8	2.84×10^8	2.88×10^8	2.904×10^{-2}	2.980×10^{-2}	0.045058
10 − 5	5.117×10^5	5.88×10^5	1.52×10^5	9.913×10^{-5}	2.950×10^{-5}	0.000214
11 − 3	8.015×10^9	7.84×10^9	7.92×10^9	1.314×10^0	1.340×10^0	2.022700
11 − 4	2.618×10^9	2.56×10^9	2.60×10^9	4.356×10^{-1}	4.480×10^{-1}	0.675718
11 − 5	7.418×10^5	7.91×10^5	1.15×10^5	2.392×10^{-4}	3.710×10^{-5}	0.000517
12 − 4	1.048×10^{10}	1.02×10^{10}	1.04×10^{10}	2.439×10^0	2.510×10^0	3.781547
13 − 3	4.347×10^6	9.07×10^6	5.79×10^6	1.327×10^{-4}	2.030×10^{-4}	0.000197
13 − 5	8.643×10^9	6.98×10^9	6.97×10^9	5.047×10^{-1}	4.840×10^{-1}	1.036879
14 − 3	9.459×10^6	9.90×10^6	1.40×10^6	9.546×10^{-4}	1.590×10^{-4}	0.001153
14 − 4	4.427×10^5	4.77×10^5	4.47×10^5	4.521×10^{-5}	5.130×10^{-5}	0.000055
14 − 5	2.085×10^{10}	1.90×10^{10}	1.88×10^{10}	3.506×10^0	3.540×10^0	5.466647

We present our collision strengths from the lowest five levels to the first 14 levels in Table 3 at electron energy values 7.779, 13.674, and 23.336 Ry. We compared them with the 5-configurations collision strengths of Christensen et al. [26]. Some important discrepancies exist for transitions involving levels arising from the 3p^3 configuration (levels 7, 8, and 9). Except for these transitions, the agreement (averaged over the three energies and all the other transitions) is about 20%. The agreement between our results and those of [26] is the worse for the electron energy 7.779 Ry. This energy is close to the excitation energy of the last calculated level (here the energy 6.80 Ry of the level 38). In this situation, the contribution of

elastic collisions (which are mostly due to close/strong collisions) is important. We remark also that the agreement is better for transitions from higher levels: for example, $\Delta\Omega_{ij}$ is about 39% for transitions from the level $i = 1$, and it is about 15% for transitions from the levels $i = 4, 5$. We note that, in [26], calculations have been carried out for partial waves $l \leq 11$. This may be the origin of the above disagreement for some transitions (we have taken into account partial waves up to 50 in the present work). The difference in the configurations number may also affect the collision strength values.

Table 3. Our collision strengths Ω_{ij} (Present) and those from [26] (DW86) where $1 \leq i \leq 5$ and $i + 1 \leq j \leq 14$. i and j label the levels as in Table 1.

$i - j$	7.779 Ry		13.674 Ry		23.336 Ry	
	Present	**DW86**	**Present**	**DW86**	**Present**	**DW86**
1 − 2	8.901×10^{-3}	9.29×10^{-3}	4.523×10^{-3}	4.54×10^{-3}	2.067×10^{-3}	2.01×10^{-3}
1 − 3	2.936×10^{-2}	2.87×10^{-2}	1.652×10^{-2}	1.46×10^{-2}	9.202×10^{-3}	7.08×10^{-3}
1 − 4	4.430×10^{-2}	4.64×10^{-2}	2.251×10^{-2}	2.26×10^{-2}	1.029×10^{-2}	1.00×10^{-2}
1 − 5	8.841×10^{0}	8.60×10^{0}	9.848×10^{0}	1.03×10^{1}	1.006×10^{1}	1.21×10^{1}
1 − 6	4.208×10^{-1}	3.57×10^{-1}	4.712×10^{-1}	3.48×10^{-1}	5.067×10^{-1}	3.17×10^{-1}
1 − 7	5.400×10^{-5}	1.06×10^{-4}	2.900×10^{-5}	5.40×10^{-5}	1.200×10^{-5}	2.33×10^{-5}
1 − 8	1.560×10^{-4}	2.81×10^{-4}	8.400×10^{-5}	1.30×10^{-4}	3.300×10^{-5}	4.64×10^{-5}
1 − 9	4.102×10^{-3}	5.74×10^{-3}	4.449×10^{-3}	5.38×10^{-3}	4.785×10^{-3}	4.80×10^{-3}
1 − 10	2.239×10^{-2}	2.39×10^{-2}	1.051×10^{-2}	1.10×10^{-2}	4.603×10^{-3}	4.73×10^{-3}
1 − 11	3.731×10^{-2}	3.99×10^{-2}	1.752×10^{-2}	1.84×10^{-2}	7.671×10^{-3}	7.87×10^{-3}
1 − 12	5.222×10^{-2}	5.58×10^{-2}	2.452×10^{-2}	2.57×10^{-2}	1.074×10^{-2}	1.10×10^{-2}
1 − 13	3.460×10^{-4}	1.28×10^{-2}	1.030×10^{-4}	1.10×10^{-2}	5.800×10^{-5}	8.06×10^{-3}
1 − 14	5.431×10^{-1}	7.40×10^{-1}	6.408×10^{-1}	8.03×10^{-1}	7.164×10^{-1}	8.46×10^{-1}
2 − 3	6.257×10^{-2}	9.55×10^{-2}	3.113×10^{-2}	5.28×10^{-2}	1.475×10^{-2}	3.03×10^{-2}
2 − 4	3.621×10^{-1}	2.98×10^{-1}	3.562×10^{-1}	2.79×10^{-1}	3.553×10^{-1}	2.50×10^{-1}
2 − 5	1.103×10^{-2}	1.19×10^{-2}	5.152×10^{-3}	5.09×10^{-3}	2.222×10^{-3}	2.13×10^{-3}
2 − 6	2.860×10^{-2}	2.77×10^{-2}	1.381×10^{-2}	1.40×10^{-2}	5.991×10^{-3}	6.05×10^{-3}
2 − 7	5.657×10^{-3}	2.09×10^{-2}	2.784×10^{-3}	2.95×10^{-3}	1.210×10^{-3}	1.27×10^{-3}
2 − 8	3.379×10^{0}	3.32×10^{0}	3.796×10^{0}	4.05×10^{0}	3.867×10^{0}	4.70×10^{0}
2 − 9	4.773×10^{-3}	6.85×10^{-2}	2.338×10^{-3}	6.45×10^{-3}	1.012×10^{-3}	3.57×10^{-3}
2 − 10	2.744×10^{0}	2.75×10^{0}	3.272×10^{0}	3.43×10^{0}	3.563×10^{0}	4.10×10^{0}
2 − 11	2.286×10^{-2}	4.89×10^{-2}	1.027×10^{-2}	1.23×10^{-2}	4.178×10^{-3}	5.19×10^{-3}
2 − 12	5.517×10^{-2}	6.10×10^{-2}	5.424×10^{-2}	5.58×10^{-2}	5.713×10^{-2}	5.14×10^{-2}
2 − 13	1.746×10^{-3}	1.68×10^{-3}	8.200×10^{-4}	9.19×10^{-4}	3.490×10^{-4}	3.75×10^{-4}
2 − 14	9.861×10^{-3}	1.25×10^{-2}	4.171×10^{-3}	4.77×10^{-3}	1.639×10^{-3}	1.85×10^{-3}
3 − 4	8.916×10^{-1}	7.87×10^{-1}	8.398×10^{-1}	6.89×10^{-1}	8.177×10^{-1}	5.96×10^{-1}
3 − 5	3.383×10^{-2}	3.61×10^{-2}	1.603×10^{-2}	1.55×10^{-2}	7.172×10^{-3}	6.55×10^{-3}
3 − 6	1.349×10^{-1}	1.43×10^{-1}	9.775×10^{-2}	1.19×10^{-1}	7.539×10^{-2}	1.10×10^{-1}
3 − 7	3.379×10^{0}	3.51×10^{0}	3.926×10^{0}	4.27×10^{0}	4.410×10^{0}	4.89×10^{0}
3 − 8	2.556×10^{0}	2.67×10^{0}	2.857×10^{0}	3.12×10^{0}	2.904×10^{0}	3.60×10^{0}
3 − 9	4.186×10^{0}	4.06×10^{0}	4.695×10^{0}	4.81×10^{0}	4.780×10^{0}	5.63×10^{0}
3 − 10	2.088×10^{0}	2.17×10^{0}	2.467×10^{0}	2.66×10^{0}	2.677×10^{0}	3.15×10^{0}
3 − 11	6.232×10^{0}	6.04×10^{0}	7.416×10^{0}	7.47×10^{0}	8.072×10^{0}	9.00×10^{0}
3 − 12	1.428×10^{-1}	1.90×10^{-1}	1.231×10^{-1}	1.28×10^{-1}	1.202×10^{-1}	1.09×10^{-1}
3 − 13	6.369×10^{-3}	6.50×10^{-3}	3.504×10^{-3}	4.24×10^{-3}	2.005×10^{-3}	2.75×10^{-3}
3 − 14	3.305×10^{-2}	3.80×10^{-2}	1.675×10^{-2}	1.49×10^{-2}	9.606×10^{-3}	6.27×10^{-3}
4 − 5	5.693×10^{-2}	6.08×10^{-2}	2.671×10^{-2}	2.61×10^{-2}	1.169×10^{-2}	1.10×10^{-2}
4 − 6	2.318×10^{-1}	2.89×10^{-1}	1.793×10^{-1}	2.75×10^{-1}	1.471×10^{-1}	2.74×10^{-1}
4 − 7	6.345×10^{-3}	7.20×10^{-2}	3.119×10^{-3}	7.70×10^{-3}	1.355×10^{-3}	4.21×10^{-3}
4 − 8	4.238×10^{0}	4.63×10^{0}	4.751×10^{0}	5.46×10^{0}	4.835×10^{0}	6.23×10^{0}
4 − 9	1.261×10^{1}	1.27×10^{1}	1.414×10^{1}	1.52×10^{1}	1.439×10^{1}	1.76×10^{1}
4 − 10	2.468×10^{-1}	2.79×10^{-1}	2.679×10^{-1}	2.93×10^{-1}	2.979×10^{-1}	3.16×10^{-1}
4 − 11	2.208×10^{0}	2.29×10^{0}	2.581×10^{0}	2.75×10^{0}	2.795×10^{0}	3.23×10^{0}
4 − 12	1.165×10^{1}	1.07×10^{1}	1.382×10^{1}	1.32×10^{1}	1.501×10^{1}	1.62×10^{1}
4 − 13	1.042×10^{-2}	1.01×10^{-2}	4.917×10^{-3}	5.27×10^{-3}	2.094×10^{-3}	2.16×10^{-3}
4 − 14	4.929×10^{-2}	6.27×10^{-2}	2.100×10^{-2}	2.39×10^{-2}	8.410×10^{-3}	9.45×10^{-3}
5 − 6	6.396×10^{0}	6.54×10^{0}	6.502×10^{0}	7.69×10^{0}	6.069×10^{0}	8.82×10^{0}
5 − 7	1.214×10^{-2}	1.21×10^{-2}	6.841×10^{-3}	8.61×10^{-3}	3.973×10^{-3}	5.89×10^{-3}
5 − 8	3.337×10^{-2}	2.99×10^{-2}	1.671×10^{-2}	1.68×10^{-2}	7.776×10^{-3}	7.31×10^{-3}
5 − 9	1.169×10^{-1}	1.34×10^{-1}	8.954×10^{-2}	1.27×10^{-1}	7.004×10^{-2}	1.27×10^{-1}
5 − 10	4.295×10^{-2}	4.18×10^{-2}	1.955×10^{-2}	1.84×10^{-2}	8.514×10^{-3}	7.74×10^{-3}
5 − 11	7.151×10^{-2}	6.94×10^{-2}	3.279×10^{-2}	3.04×10^{-2}	1.459×10^{-2}	1.25×10^{-2}
5 − 12	9.742×10^{-2}	9.63×10^{-2}	4.322×10^{-2}	4.18×10^{-2}	1.770×10^{-2}	1.69×10^{-2}
5 − 13	3.939×10^{0}	4.46×10^{0}	4.478×10^{0}	5.32×10^{0}	4.587×10^{0}	6.12×10^{0}
5 − 14	1.653×10^{1}	1.64×10^{1}	1.990×10^{1}	2.06×10^{1}	2.181×10^{1}	2.54×10^{1}

3.2. Line Broadening Results

Two methods for line broadening calculations have been used in our work. The first is the quantum mechanical approach (Q), and the second is the semiclassical perturbation method SCP. To evaluate the line broadening through the second method, we need atomic parameters such as energy levels and oscillator strengths. In our SCP calculations (SCP_{SST}), we have taken atomic data of the code SST [14]. We compare our results (Q and SCP_{SST}) to the SCP calculations (SCP_{BD}) performed in [12], where atomic data have been taken from the method of Bates and Damgaard [13]. This method has been used many times with different ions, and it has been shown that the corresponding results (using the Bates and Damgaard or the SST data) are in good agreement with experimental and other theoretical results [31–33]. Many of these SCP results have been stored in the database STARK-B [34].

We have performed quantum (Q) and semiclassical perturbation (SCP) Stark broadening for 12 lines of Ar VII for electron temperature range $(2 - 50) \times 10^4$ K and at electron density $N_e = 10^{18}$ cm^{-3}. We present our results in Table 4 for transitions between singlets, in Table 5 for the resonance line $3s^2$ $^1S_0 - 3s3p$ $^1P_1^o$, and in Table 6 for transitions between triplets. A comparison was made between our quantum and our semiclassical perturbation results SCP_{SST} in Tables 4 and 5. We also included the semiclassical results SCP_{BD} [12] in Table 6 in our comparison. Tables 4 and 6 show that the quantum line widths are always higher than the two semiclassical ones (SCP_{SST} and SCP_{BD}). We also found that, except for the resonance line, the ratio $\frac{Q}{SCP}$ increases and decreases with temperature. The decreasing part starts in general at $T \simeq 10^5$ K. For the resonance line $3s^2$ $^1S_0 - 3s3p$ $^1P_1^o$, the ratio $\frac{Q}{SCP}$ increases with T. As per Table 5, this ratio has the same behavior as that of the other lines (increasing and after decreasing) but starts to decrease for higher temperatures ($T \simeq 10^6$ K). Table 6 shows that, in all studied cases, the SCP_{SST} widths are closer to the quantum results than the SCP_{BD} ones. The disagreement between SCP_{SST} and SCP_{BD} results is due to the difference in the source of the used atomic data.

To understand the difference between SCP and quantum calculations, we present also, in Tables 4 and 6, the contributions of elastic ($\frac{Elastic}{Total}$) and strong ($\frac{Strong}{Total}$) collisions to the SCP_{SST} line broadening. Firstly, we remark that, for $T > 10^5$ K and except the resonance line, the ratios $\frac{Elastic}{Total}$ and $\frac{Strong}{Total}$ decrease with the temperature. Secondly, we see that, for each line, as the elastic and strong collisions contributions decrease, the two results (Q and SCP) become close to each other. For electron temperature $T \leq 5 \times 10^4$ K, we can detect in some cases an opposite behavior between $\frac{Elastic}{Total}$ and $\frac{Strong}{Total}$ on the one hand and the ratio $\frac{Q}{SCP}$ on the other hand. This may be due to the contributions of resonances that are dominant at low temperatures. These contributions are taken into account differently in the quantum and the semiclassical perturbative methods. Figure 1 shows the behavior of the ratios $\frac{Q}{SCP}$ and $\frac{Strong}{Total}$ with the electron temperature for the $3s3d$ $^3D_2 - 3s4p$ $^3P_1^o$, $3s3p$ $^3P_2^o - 3s4d$ $^3D_3$, $3s4p$ $^3P_2^o - 3s4d$ $^3D_3$, and $3s3p$ $^1P_1^o - 3s4s$ $^1S_0$ transitions. In fact, the Ar VII perturbing levels i' and f' are so far from the initial (i) and final (f) levels of the considered transition ($\Delta E_{ii'}$ and $\Delta E_{ff'}$ are high) and, due to this fact, for collisions by electrons, the close collisions are important. Furthermore, with the used temperature values, the ratio $\Delta E / k_B T$ is high and consequently, the inelastic cross sections are small compared to the elastic ones that become dominant (mostly due to the close collisions). The perturbative treatment in the semiclassical approach does not correctly estimate this contribution. In that situation, it is necessary to perform more sophisticated calculations such as the quantum ones. We have shown in Elabidi et al. [11], through extensive comparisons between quantum and semiclassical Stark broadening of Ar XV lines, that the disagreement between the two results increases with the increase in strong collision contributions. Figure 2 displays the Stark widths as a function of the electron temperature at a constant electron density for two selected lines between singlets : $3s^2$ $^1S_0 - 3s4p$ $^1P_1^o$ and $3s4p$ $^1P_1^o - 3s5s$ $^1S_0$ and two lines between triplets: $3s3p$ $^3P_2^o - 3s4d$ $^3D_3$, and $3s3d$ $^3D_2 - 3s4p$ $^3P_1^o$.

The obtained Stark broadening parameters will be useful for the investigation and modeling of the plasma of stellar atmospheres. They will be also important for the investigation of laser-produced and inertial fusion plasmas.

Table 4. Our Stark line widths (FWHM) Q for Ar VII at electron density $N_e = 10^{18}$ cm^{-3} compared to the semiclassical results SCP_{SST} obtained using the atomic data of the code SST. $\frac{Elastic}{Total}$ and $\frac{Strong}{Total}$ are respectively the contributions of elastic and strong collisions to SCP line broadening. T is expressed in 10^4 K.

Transition	T	Q (Å)	SCP_{SST}	$\frac{Elastic}{Total}$	$\frac{Strong}{Total}$	$\frac{Q}{SCP}$
3s^2 ^{1}S$_0$−3s3p ^{1}P$_1^o$ $\lambda = 585.75$ Å	2	2.684×10^{-2}	2.380×10^{-2}	0.966	0.288	1.13
	5	1.872×10^{-2}	1.500×10^{-2}	0.937	0.287	1.25
	10	1.453×10^{-2}	1.070×10^{-2}	0.891	0.286	1.36
	20	1.135×10^{-2}	7.640×10^{-3}	0.789	0.282	1.49
	30	9.875×10^{-3}	6.360×10^{-3}	0.706	0.276	1.55
	50	8.322×10^{-3}	5.160×10^{-3}	0.605	0.267	1.61
3s^2 ^{1}S$_0$−3s4p ^{1}P$_1^o$ $\lambda = 175.5$ Å	2	9.941×10^{-3}	6.070×10^{-3}	0.897	0.575	1.64
	5	6.242×10^{-3}	2.930×10^{-3}	0.827	0.361	2.13
	10	4.370×10^{-3}	2.110×10^{-3}	0.766	0.357	2.07
	20	3.038×10^{-3}	1.550×10^{-3}	0.689	0.345	1.96
	30	2.445×10^{-3}	1.320×10^{-3}	0.641	0.334	1.85
	50	1.848×10^{-3}	1.090×10^{-3}	0.588	0.319	1.70
3s3p ^{1}P$_1^o$−3s4s ^{1}S$_0$ $\lambda = 279.2$ Å	2	6.322×10^{-2}	9.750×10^{-3}	0.944	0.155	6.48
	5	3.923×10^{-2}	5.400×10^{-3}	0.767	0.175	7.26
	10	2.676×10^{-2}	3.190×10^{-3}	0.616	0.172	6.84
	20	1.759×10^{-2}	2.920×10^{-3}	0.472	0.162	6.02
	30	1.344×10^{-2}	2.500×10^{-3}	0.401	0.155	5.38
	50	9.332×10^{-3}	2.080×10^{-3}	0.328	0.145	4.49
3s4p ^{1}P$_1^o$−3s5s ^{1}S$_0$ $\lambda = 662.6$ Å	2	4.517×10^{-1}	1.360×10^{-1}	0.792	0.193	3.32
	5	2.942×10^{-1}	8.840×10^{-2}	0.595	0.189	3.33
	10	1.975×10^{-1}	6.570×10^{-2}	0.458	0.179	3.01
	20	1.266×10^{-1}	5.050×10^{-2}	0.359	0.166	2.51
	30	9.671×10^{-2}	4.400×10^{-2}	0.315	0.156	2.20
	50	6.843×10^{-2}	3.740×10^{-2}	0.274	0.144	1.83
3s3d ^{1}D$_2$−3s4p ^{1}P$_1^o$ $\lambda = 489.6$ Å	2	1.910×10^{-1}	4.150×10^{-2}	0.859	0.361	4.60
	5	1.355×10^{-1}	2.650×10^{-2}	0.809	0.356	5.11
	10	1.011×10^{-1}	1.930×10^{-2}	0.737	0.346	5.24
	20	6.854×10^{-2}	1.430×10^{-2}	0.661	0.335	4.79
	30	5.206×10^{-2}	1.210×10^{-2}	0.611	0.323	4.30
	50	3.602×10^{-2}	1.010×10^{-2}	0.561	0.307	3.57
3s3p ^{1}P$_1^o$−3s5s ^{1}S$_0$ $\lambda = 176.5$ Å	2	1.779×10^{-2}	8.070×10^{-3}	0.825	0.085	2.20
	5	1.119×10^{-2}	4.750×10^{-3}	0.559	0.092	2.36
	10	7.845×10^{-3}	3.520×10^{-3}	0.400	0.087	2.23
	20	5.460×10^{-3}	2.710×10^{-3}	0.282	0.081	2.01
	30	4.390×10^{-3}	2.360×10^{-3}	0.229	0.076	1.86
	50	3.303×10^{-3}	2.000×10^{-3}	0.177	0.069	1.65

Table 5. Our Stark widths (FWHM) Q for the Ar VII $3s^2\,^1S_0-3s3p\,^1P_1^o$ resonance line at electron density $N_e = 10^{18}$ cm^{-3} compared to the semiclassical results SCP_{SST} obtained using the atomic data of the code SST. $\frac{Elastic}{Total}$ and $\frac{Strong}{Total}$ are respectively the contributions of elastic and strong collisions to SCP line broadening. T is expressed in 10^5 K.

Transition	T	Q (Å)	SCP_{SST}	$\frac{Elastic}{Total}$	$\frac{Strong}{Total}$	$\frac{Q}{SCP}$
	0.2	2.684×10^{-2}	2.380×10^{-2}	0.966	0.288	1.13
	0.5	1.872×10^{-2}	1.500×10^{-2}	0.937	0.287	1.25
	1	1.453×10^{-2}	1.070×10^{-2}	0.891	0.286	1.36
	2	1.135×10^{-2}	7.640×10^{-3}	0.789	0.282	1.49
$3s^2\,^1S_0-3s3p\,^1P_1^o$	3	9.875×10^{-3}	6.360×10^{-3}	0.706	0.276	1.55
$\lambda = 585.75$ Å	5	8.322×10^{-3}	5.160×10^{-3}	0.605	0.267	1.61
	7.5	7.271×10^{-3}	4.430×10^{-3}	0.537	0.255	1.64
	10	6.593×10^{-3}	4.020×10^{-3}	0.494	0.245	1.64
	15	5.699×10^{-3}	3.530×10^{-3}	0.444	0.232	1.61
	30	4.284×10^{-3}	2.890×10^{-3}	0.389	0.211	1.48
	50	3.327×10^{-3}	2.530×10^{-3}	0.366	0.199	1.32

Table 6. Same as in Table 4 but we add the semiclassical results SCP_{BD} obtained in Dimitrijević et al. [12] using the atomic data from Bates and Damgaard [13]. Electron density is $N_e = 10^{18}$ cm^{-3} and T is expressed in 10^4 K.

Transition	T	Q	SCP_{SST}	SCP_{BD}	$\frac{Q}{SCP_{SST}}$	$\left(\frac{Elastic}{Total}\right)_{SST}$	$\left(\frac{Strong}{Total}\right)_{SST}$	$\frac{Q}{SCP_{BD}}$
	2	7.510×10^{-3}	4.83×10^{-3}	4.21×10^{-3}	1.55	0.889	0.444	1.77
	5	4.748×10^{-3}	2.86×10^{-3}	2.49×10^{-3}	1.66	0.877	0.475	1.90
$3s3p\,^3P_2^o-3s4d\,^3D_3$	10	3.369×10^{-3}	2.04×10^{-3}	1.81×10^{-3}	1.65	0.861	0.472	1.85
$\lambda = 192.3$ Å	20	2.389×10^{-3}	1.48×10^{-3}	1.35×10^{-3}	1.62	0.823	0.461	1.77
	30	1.967×10^{-3}	1.25×10^{-3}	1.15×10^{-3}	1.47	0.798	0.453	1.70
	50	1.532×10^{-3}	1.02×10^{-3}	9.51×10^{-4}	1.50	0.764	0.437	1.61
	2	1.613×10^{0}	3.76×10^{-1}	3.09×10^{-1}	4.29	0.901	0.457	5.22
	5	1.061×10^{0}	2.38×10^{-1}	1.99×10^{-1}	4.46	0.873	0.455	5.33
$3s4p\,^3P_2^o-3s4d\,^3D_3$	10	7.141×10^{-1}	1.71×10^{-1}	1.45×10^{-1}	4.18	0.824	0.448	4.92
$\lambda = 1425.9$ Å	20	4.285×10^{-1}	1.26×10^{-1}	1.08×10^{-1}	3.40	0.767	0.435	3.97
	30	3.073×10^{-1}	1.07×10^{-1}	9.27×10^{-2}	2.87	0.740	0.424	3.31
	50	2.013×10^{-1}	8.87×10^{-2}	7.77×10^{-2}	2.27	0.705	0.406	2.59
	2	7.585×10^{-2}	2.33×10^{-2}	1.84×10^{-2}	3.26	0.928	0.406	4.12
	5	4.562×10^{-2}	1.52×10^{-2}	1.16×10^{-2}	3.00	0.878	0.397	3.93
$3s3d\,^3D_2-3s4p\,^3P_1^o$	10	2.896×10^{-2}	1.10×10^{-2}	8.35×10^{-3}	2.64	0.809	0.389	3.47
$\lambda = 416.0$ Å	20	1.806×10^{-2}	8.14×10^{-3}	6.12×10^{-3}	2.22	0.723	0.375	2.95
	30	1.389×10^{-2}	6.91×10^{-3}	5.18×10^{-3}	2.01	0.675	0.364	2.68
	50	1.040×10^{-2}	5.73×10^{-3}	4.27×10^{-3}	1.82	0.625	0.346	2.43
	2	7.605×10^{-1}	5.36×10^{-1}	5.34×10^{-1}	1.42	0.942	0.337	1.42
	5	5.453×10^{-1}	3.44×10^{-1}	3.33×10^{-1}	1.59	0.863	0.331	1.64
$3s4s\,^3S_1-3s4p\,^3P_1^o$	10	4.272×10^{-1}	2.49×10^{-1}	2.40×10^{-1}	1.72	0.757	0.326	1.78
$\lambda = 1982.0$ Å	20	3.336×10^{-1}	1.85×10^{-1}	1.79×10^{-1}	1.80	0.632	0.309	1.86
	30	2.871×10^{-1}	1.59×10^{-1}	1.53×10^{-1}	1.81	0.577	0.298	1.88
	50	2.350×10^{-1}	1.33×10^{-1}	1.28×10^{-1}	1.77	0.518	0.281	1.84
	2	1.396×10^{-2}	8.72×10^{-3}	5.06×10^{-3}	1.56	0.996	0.358	2.75
	5	8.893×10^{-3}	5.35×10^{-3}	2.68×10^{-3}	1.66	0.947	0.368	3.30
$3s3p\,^3P_2^o-3s4s\,^3S_1$	10	6.351×10^{-3}	3.80×10^{-3}	1.91×10^{-3}	1.67	0.860	0.368	3.31
$\lambda = 250.4$ Å	20	4.549×10^{-3}	2.78×10^{-3}	1.41×10^{-3}	1.64	0.750	0.358	3.21
	30	3.742×10^{-3}	2.35×10^{-3}	1.21×10^{-3}	1.59	0.690	0.349	3.08
	50	2.915×10^{-3}	1.94×10^{-3}	1.01×10^{-3}	1.50	0.626	0.333	2.87
	2	5.727×10^{-2}	1.69×10^{-2}	9.11×10^{-3}	3.39	0.986	0.334	6.24
	5	2.896×10^{-2}	9.92×10^{-3}	5.85×10^{-3}	2.92	0.961	0.363	4.91
$3s3p\,^3P_2^o-3s3d\,^3D_3$	10	1.708×10^{-2}	7.02×10^{-3}	4.17×10^{-3}	2.43	0.921	0.362	4.06
$\lambda = 477.5$ Å	20	1.022×10^{-2}	5.02×10^{-3}	2.96×10^{-3}	2.04	0.830	0.357	3.43
	30	7.755×10^{-3}	4.18×10^{-3}	2.45×10^{-3}	1.86	0.764	0.353	3.14
	50	5.734×10^{-3}	3.37×10^{-3}	1.95×10^{-3}	1.70	0.684	0.343	2.92
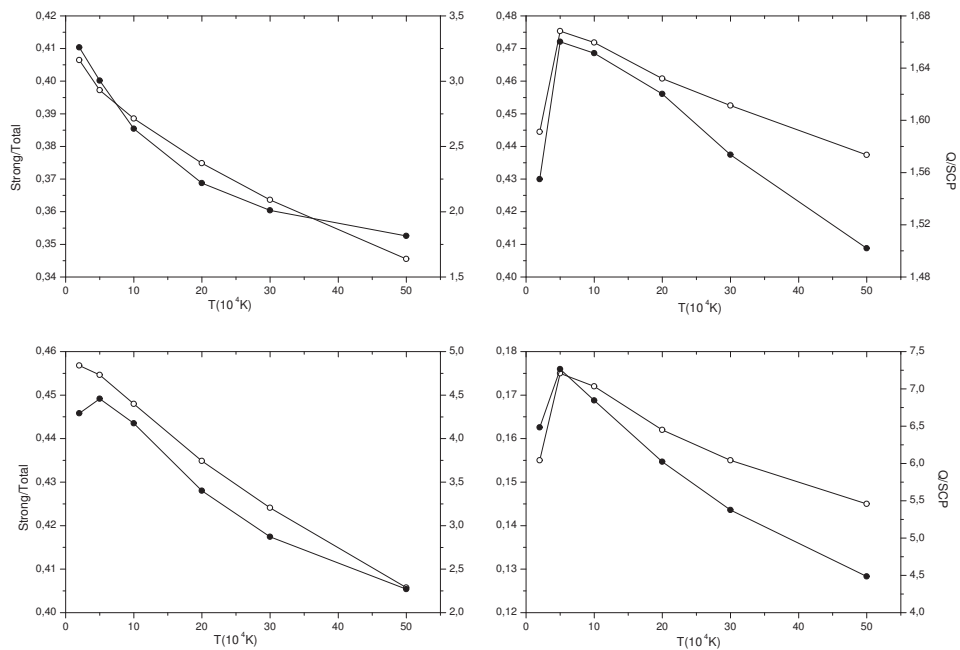
Figure 1. Ratios $\frac{Q}{SCP_{SST}}$ (●) and $\frac{Strong}{Total}$ (○) as a function of the electron temperature for the transitions: 3s3d $^3D_2-$ 3s4p $^3P_1^o$ (**left up**), 3s3p $^3P_2^o-$3s4d $^3D_3$ (**right up**), 3s4p $^3P_2^o-$3s4d $^3D_3$ (**left down**), and 3s3p $^1P_1^o-$3s4s $^1S_0$ (**right down**).
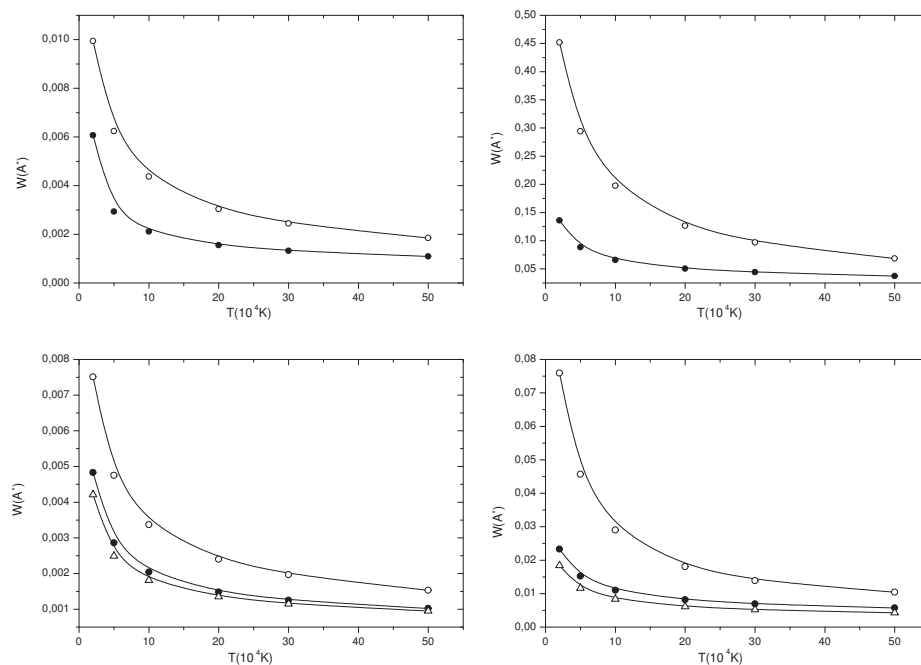
Figure 2. Stark width (FWHM) *W* as a function of the electron temperature for transitions 3s^2 $^1S_0-$3s4p $^1P_1^o$ (**left up**) and 3s4p $^1P_1^o-$3s5s $^1S_0$ (**right up**) at electron density $N_e = 10^{17}$ cm^{-3}, and for transitions 3s3p $^3P_2^o-$3s4d $^3D_3$ (**left down**) and 3s3d $^3D_2-$ 3s4p $^3P_1^o$ (**right down**) at electron density $N_e = 10^{18}$ cm^{-3}. ○: Present quantum results. ●: Present SCP results. △: SCP results from [12].

4. Conclusions

We have calculated in the present work quantum and semiclassical perturbation Stark broadening parameters for 12 Ar VII lines at electron temperatures from 2×10^4 to 5×10^5 K and at electron density $N_e = 10^{18}$ cm^{-3}. The structure and collision problem has also been treated for this ion. We have used nine configurations ($1s^2 2s^2 2p^6$: $3s^2$, $3s3p$, $3p^2$, $3s3d$, $3p3d$, $3s4s$, $3s4p$, $3s4d$, and $3s5s$). The structure and collisional parameters have been used in our quantum mechanical line broadening calculations. Since it is important to check their accuracy, we compared our energies to those of [22], to those obtained by the multiconfiguration Hartree-Fock method [24], and to those obtained from the AUTOSTRUCTURE code [25]. An acceptable agreement was found with the NIST results (better than 1%). We also compared our A_{ij} values with those obtained from the AUTOSTRUCTURE code [25] and with those from the SUPERSTRUCTURE code [26] using five configurations ($1s^2 2s^2 2p^6$: $3s^2$, $3s3p$, $3p^2$, $3s3d$, and $3s4s$). The averaged difference is about 20% with the results of [25] and about 24% with those of Christensen et al. [26]. The oscillator strengths have been compared only with the results of Christensen et al. [26], and we found an averaged agreement of about 24%. The electron-ion collision process was also studied, and collision strengths from the lowest five levels to the first 14 levels are presented at three electron energies 7.779 Ry, 13.674 Ry, and 23.336 Ry. The comparison with the collision strengths of Christensen et al. [26] indicates an agreement (averaged over the considered transitions and energies) of about 20%. The reason for the disagreement between the two results could be the difference in the number of the configurations and the difference in the partial waves taken into account in the two calculations. Stark line widths for 12 lines have been calculated using our quantum formalism. We perform also a semiclassical perturbation calculations using the structure data of the SST code. We present other semiclassical widths [12] obtained using the atomic data from Bates and Damgaard [13]. Firstly, the disagreement between the two semiclassical calculations is due to the difference in the source of atomic data. Secondly, we have shown that the disagreement between the quantum and the semiclassical widths increases with the increase in the contributions to line broadening of elastic collisions (which are mostly due to strong collisions). This is because the perturbative treatment in the semiclassical approach does not estimate very well the strong collisions. We hope that the present results can fill the lack of line broadening parameters or improve the available results for the Ar VII ion, which are of interest in the investigation and modeling of astrophysical and laboratory plasmas.

Author Contributions: R.A. and H.E. performed the calculations; H.E., S.S.B., and M.S.D. analyzed the data; H.E. wrote the paper.

Conflicts of Interest: The authors declare no conflict of interest. The founding sponsors had no role in the design of the study; in the collection, analyses, or interpretation of data; in the writing of the manuscript; or in the decision to publish the results.

References

1. Dimitrijević, M.S. Stark broadening in astrophysics (applications of Belgrade school results and collaboration with former Soviet republics. *Astron. Astrophys. Trans.* **2003**, *22*, 389–412.
2. Popović, L.Č.; Simić, S.; Milovanović N.; Dimitrijević, M.S. Stark Broadening Effect in Stellar Atmospheres: Nd II Lines. *Astrophys. J. Suppl. Ser.* **2001**, *135*, 109–114.
3. Dimitrijević, M.S.; Ryabchikova, T.; Simić, Z.; Popović, L.Č.; Dačić, M. The influence of Stark broadening on Cr II spectral line shapes in stellar atmospheres. *Astron. Astrophys.* **2007**, *469*, 681–686.

4. Rauch, T.; Ziegler, M.; Werner, K.; Kruk, J.W.; Oliveira, C.M.; Putte, D.V.; Mignani, R.P.; Kerber, F. High-resolution FUSE and HST ultraviolet spectroscopy of the white dwarf central star of Sh 2-216. *Astron. Astrophys.* **2007**, *470*, 317–329.

5. Werner, K.; Rauch, T.; Kruk, J.W. Discovery of photospheric argon in very hot central stars of planetary nebulae and white dwarfs. *Astron. Astrophys.* **2007**, *466*, 317–322.

6. Djurović, S.; Mar, S.; Peláez, R.J.; Aparicio, J.A. Stark broadening of ultraviolet Ar III spectral lines. *Mon. Not. R. Astron. Soc.* **2011**, *414*, 1389–1396.

7. Elabidi, H.; Ben Nessib, N.; Sahal-Bréchot, S. Quantum mechanical calculations of the electron-impact broadening of spectral lines for intermediate coupling. *J. Phys. B* **2004**, *37*, 63–71.

8. Elabidi, H.; Ben Nessib, N.; Cornille, M. Dubau, J.; Sahal-Bréchot, S. Electron impact broadening of spectral lines in Be-like ions: Quantum calculations. *J. Phys. B* **2008**, *41*, 025702.

9. Elabidi, H.; Sahal-Bréchot, S.; Ben Nessib, N. Quantum Stark broadening of 3s-3p spectral lines in Li-like ions; Z-scaling and comparison with semi-classical perturbation theory. *Eur. Phys. J. D* **2009**, *54*, 51–64.

10. Elabidi, H.; Sahal-Bréchot, S. Checking the dependence on the upper level ionization potential of electron impact widths using quantum calculations. *Eur. Phys. J. D* **2011**, *61*, 285–290.

11. Elabidi, H.; Sahal-Bréchot, S.; Dimitrijević, M.S. Quantum Stark broadening of Ar XV lines. Strong collision and quadrupolar potential contributions. *Adv. Res. Space* **2014**, *54*, 1184–1189.

12. Dimitrijević, M.S.; Valjarević, A.; Sahal-Bréchot, S. Semiclassical Stark broadening parameters of Ar VII spectral lines. *Atoms* **2017**, *5*, 27.

13. Bates, D.R.; Damgaard, A. The calculation of the absolute strengths of spectral lines. *Phil. Trans. R. Soc. Lond. A* **1949**, *242*, 101–122.

14. Eissner, W.; Jones, M.; Nussbaumer, H. Techniques for the calculation of atomic structures and radiative data including relativistic corrections. *Comput. Phys. Commun.* **1974**, *8*, 270–306.

15. Bethe, H.A.; Salpeter, E.E. *Quantum Mechanics of One- and Two-Electron Atoms*; Springer: Berlin/Göttingen, Germany, 1957.

16. Eissner, W. The UCL distorted wave code. *Comput. Phys. Commun.* **1998**, *114*, 295–341.

17. Saraph, H.E. Fine structure cross sections from reactance matrices. *Comput. Phys. Commun.* **1972**, *4*, 256–268.

18. Sahal-Bréchot, S. Impact Theory of the Broadening and Shift of Spectral Lines due to Electrons and Ions in a Plasma. *Astron. Astrophys.* **1969**, *1*, 91–123.

19. Sahal-Bréchot, S. Impact Theory of the Broadening and Shift of Spectral Lines due to Electrons and Ions in a Plasma (Continued). *Astron. Astrophys.* **1969**, *2*, 322–354.

20. Fleurier, C.; Sahal-Bréchot, S.; Chapelle, J. Stark profiles of some ion lines of alkaline earth elements. *J. Quant. Spectrosc. Radiat. Transfer* **1977**, *17*, 595–603.

21. Sahal-Bréchot, S.; Dimitrijević, M.S.; Ben Nessib, N. Widths and Shifts of Isolated Lines of Neutral and Ionized Atoms Perturbed by Collisions with Electrons and Ions: An Outline of the Semiclassical Perturbation Method and of the Approximations Used for the Calculations. *Atoms* **2014**, *2*, 225–252.

22. Kramida, A.; Ralchenko, Y.; Reader, J.; NIST ASD Team. *NIST Atomic Spectra Database (Version 5.5.1)*; National Institute of Standards and Technology: Gaithersburg, MD, USA, 2015. Available online: http://physics.nist.gov/asd (accessed on 8 November 2017).

23. Saloman, E.B. Energy Levels and Observed Spectral Lines of Ionized Argon, Ar II through Ar XVIII. *J. Phys. Chem. Ref. Data* **2010**, *39*, 033101.

24. Froese Fischer, C.; Tachiev, G.; Irimia, A. Relativistic energy levels, lifetimes, and transition probabilities for the sodium-like to argon-like sequences. *At. Data Nucl. Data Tables* **2006**, *92*, 607–812.

25. Fernández-Menchero, L.; Del Zanna, G.; Badnell, N.R. R-matrix electron-impact excitation data for the Mg-like iso-electronic sequence. *Astron. Astrophys.* **2014**, *572*, A115.

26. Christensen, R.B.; Norcross, D.W.; Pradhan, A.K. Electron-impact excitation of ions in the magnesium sequence. II. SV, ArVII, CaIX, CrXIII, and NiXVII. *Phys. Rev. A* **1986**, *34*, 4704–4715.

27. Del Zanna, G.; Dere, K.P.; Young, P.R.; Landi, E.; Mason, H.E. CHIANTI—An atomic database for emission lines. *Astron. Astrophys.* **2015**, *582*, A56.

28. Burgess, A.; Sheorey, V.B. Electron impact excitation of the resonance lines of alkali-like positive ions. *J. Phys. B* **1974**, *7*, 2403–2416.

29. Chidichimo, M.C.; Haig, S.P. Electron-impact excitation of quadrupole-allowed transitions in positive ions. *Phys. Rev. A* **1989**, *39*, 4991–4997.

30. Chidichimo, M.C. Electron-impact excitation of electric octupole transitions in positive ions: Asymptotic behavior of the sum over partial-collision strengths. *Phys. Rev. A* **1992**, *45*, 1690–1700.

31. Hamdi, R.; Ben Nessib, N.; Dimitrijević, M.S.; Sahal-Bréchot, S. Stark broadening of Pb IV lines. *Mon. Not. R. Astron. Soc.* **2013**, *431*, 1039–1047.

32. Hamdi, R.; Ben Nessib, N.; Sahal-Bréchot, S.; Dimitrijević, M.S. Stark widths of Ar III spectral lines in the atmospeheres of subdwarfs B stars. *Adv. Res. Space* **2014**, *54*, 1223–1230.

33. Hamdi, R.; Ben Nessib, N.; Sahal-Bréchot, S.; Dimitrijević, M.S. Stark widths of Ar II spectral lines in the atmospeheres of subdwarfs B stars. *Atoms* **2017**, *5*, 26.

34. Sahal-Bréchot, S.; Dimitrijević, M.S.; Moreau, N. STARK-B Database. Observatory of Paris, LERMA and Astronomical Observatory of Belgrade, 2017. Available online: http://stark-b.obspm.fr (accessed on 8 November 2017).